

I. Neri<sup>1,4</sup>, M. Emendi<sup>1</sup>, C. Canevari<sup>1</sup>, A. Savi<sup>1</sup>, V. Bettinardi<sup>1</sup>, C. Losio<sup>2</sup>, E. Venturini<sup>2</sup>, R. Menichini<sup>1</sup>, L. Presotto<sup>1</sup>, R. Di Micco<sup>3</sup>, O. D. Gentilini<sup>3</sup>, M. Picchio<sup>1,4</sup>, L. Gianolli<sup>1</sup>, P. Scifo<sup>1</sup>

<sup>1</sup>Nuclear Medicine Dept., San Raffaele Hospital, Milan, Italy; <sup>2</sup>Radiology Dept., IRCCS San Raffaele Scientific Institute, Milan, Italy; <sup>3</sup>Breast Surgery Unit Dept., IRCCS San Raffaele Scientific Institute, Milan, Italy; <sup>4</sup>Vita-Salute San Raffaele University, Milan, Italy.

## INTRODUCTION

Hybrid PET/MRI (Positron Emission Tomography/Magnetic Resonance Imaging) is an innovative technique that allows to combine morphologic and functional data offering a ground-breaking non-invasive approach to cancer detection and characterization, reaching high levels of accuracy [1], [2]. Reliable estimation of PET attenuation correction (AC) based on MRI is a fundamental issue in PET/MRI. The standard MR-based method for generating AC-maps in the body is the segmentation of a two-point DIXON sequence into different tissue classes (i.e. soft-tissue, fat, lung and air) and then assigning AC values (single or continuous values) to each class [3], [4]. Breast PET/MR examination includes a one-FOV (Field Of View) acquisition in prone position using the coil specific for the breast. Due to the patient's prone position and the limited FOV in MR imaging, truncations in body imaging occur and can lead to the generation of incomplete MR-based AC-maps [5], [6]. In this preliminary work, we aim to investigate how, modifying some specific acquisition parameters (spatial resolution and SNR) of the MR sequence for AC (MRAC), PET images are affected both quantitatively and qualitatively.

## SUBJECTS AND METHODS

Forty-six women (mean age: 50.44±12.7ys) with breast cancer underwent 18F-FDG PET/MR study using the 3T SIGNA PET/MR (General Electric Healthcare, Waukesha, WI, US) scanner. During breast prone PET scan, standard MRAC acquisition (pixel size 1.95mmx1.95mm, matrix 256x128, 120 slices, slice thickness 2.6mm, FOV=50cmx50cm, TR/TE=4ms/1.7ms, NEX=0.7) has been collected. Additionally, five different MRAC sequences were acquired with the same parameters of the standard MRAC (Ref) except for: A) NEX=1; B) matrix 256x256, NEX=1; C) NEX=2; D) matrix 256x256, NEX=2; E) improved dorsal region localized shimming. Axial T2w FSE, DWI and 3D Multi phase Vibrant with Gd-injection were also acquired during PET scan. Using offline GE Duetto Toolbox, six PET reconstructed images were obtained correcting attenuation with different MRACs (Fig.1). Common reconstruction parameters to all the reconstruction set were: Algorithm = OSEM, number of subsets=28, number of iteration=2, Post\_Gaussian Filter=4 mm FWHM, Axial Filter=Standard, PSF, with truncation correction obtained from TOFNAC acquisition.

An expert Nuclear Medicine physician defined the volumes of interest on the breast lesions (BL) and lymph nodes (LN) on the PET reconstructed images (using the standard MRAC - Ref).  $SUV_{max}$  and  $SUV_{mean}$  were calculated together with the percentage differences ( $SUV_{diff}$ ) and the Root Mean Squared Error (RMSE) between the new set of images and the reference.

Figure 1

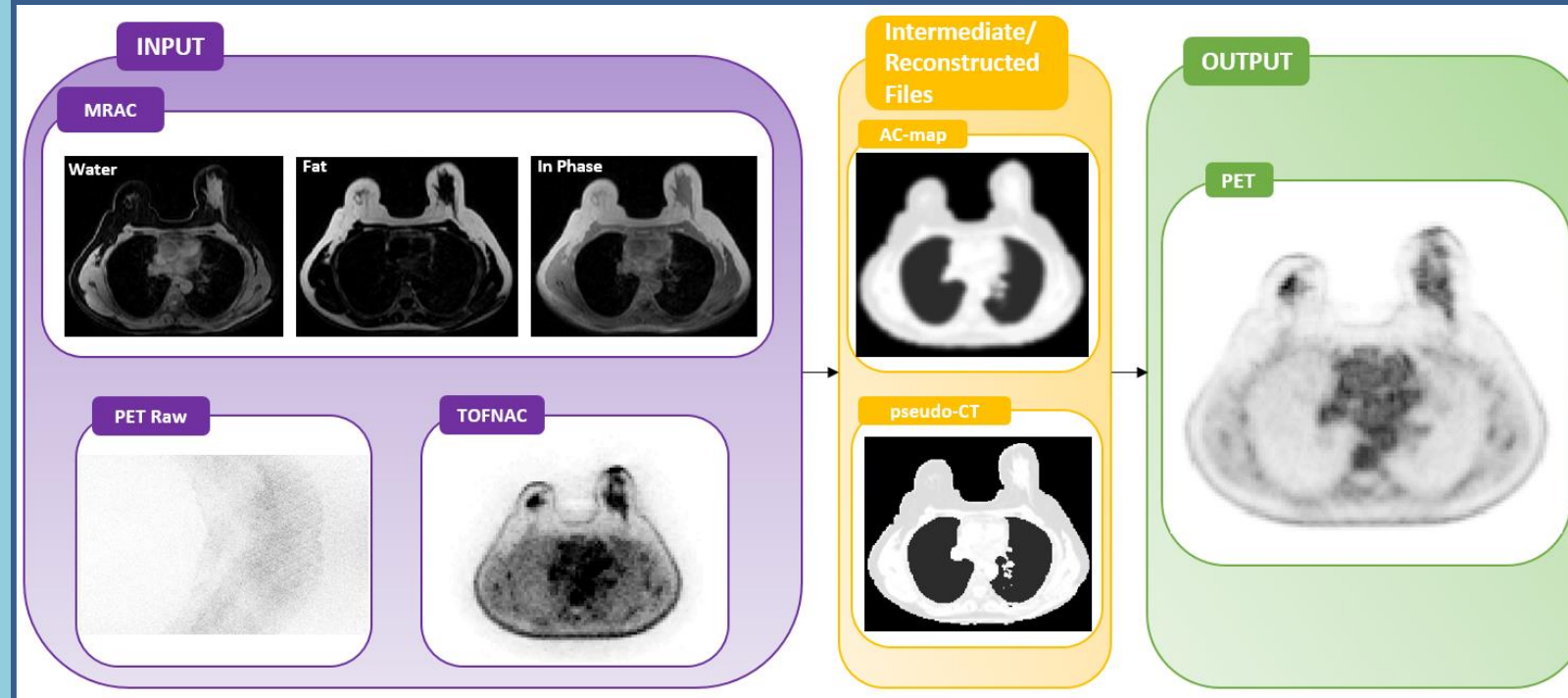


Fig. 1. Brief Duetto Toolbox workflow.

Figure 2

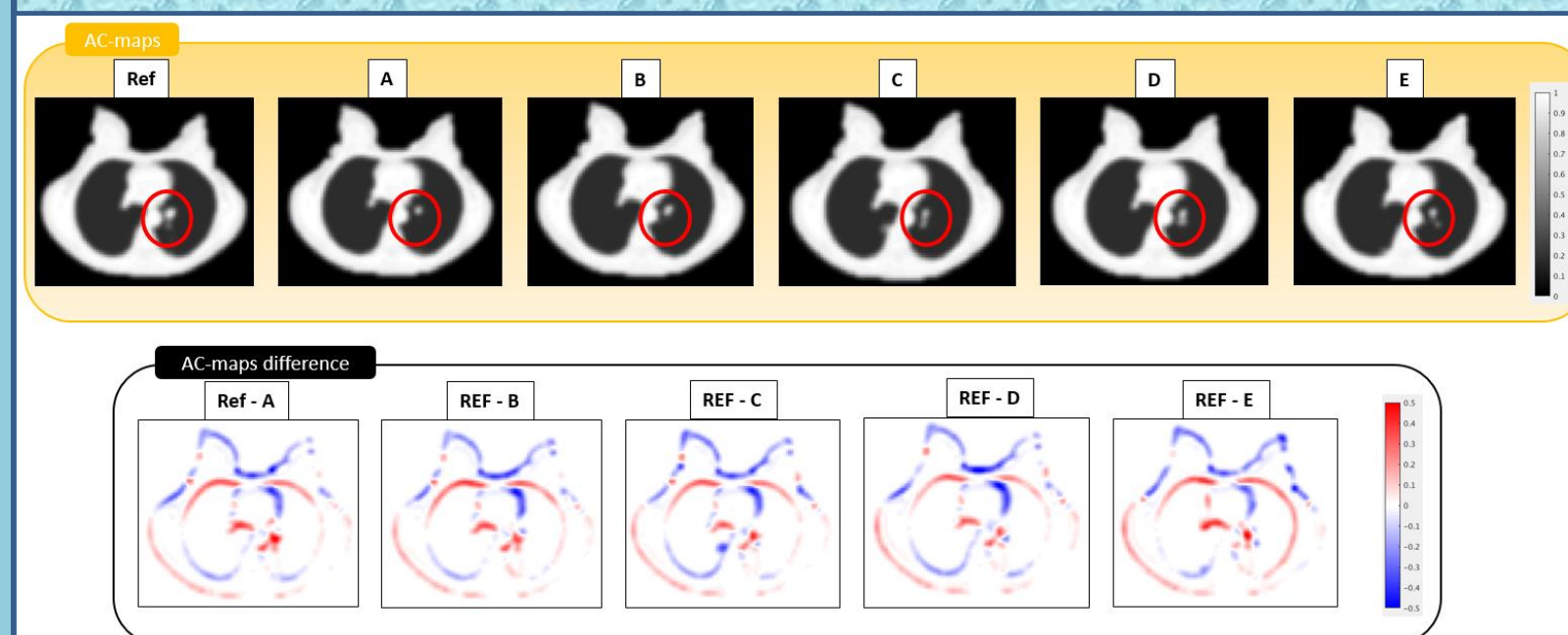


Fig. 2. Example of AC-maps obtained from each set of acquisition parameters and the subtraction between them and the reference one (respectively, in the upper and in the lower row).

Figure 3

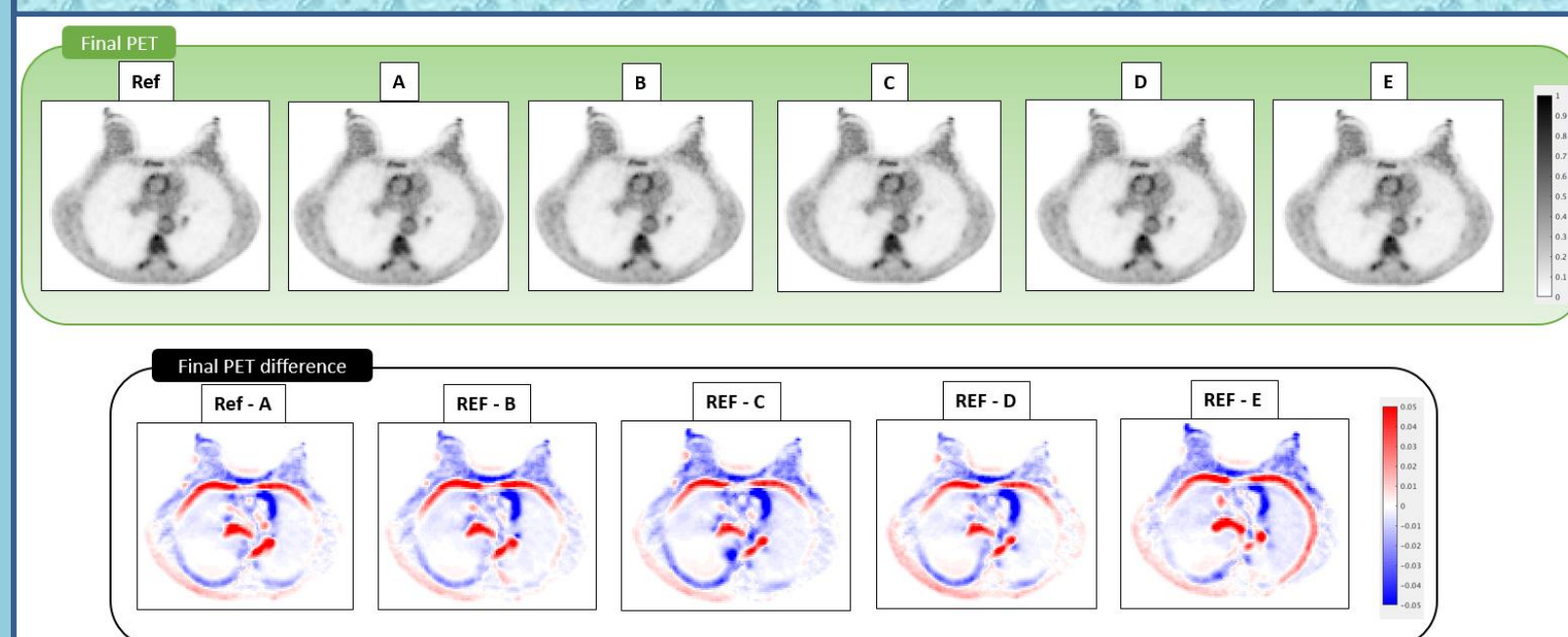


Fig. 3. Example of the final PET image, reconstructed from different AC-maps. The six PET images and the maps of the subtraction between the reference PET image and the other five ones are shown (respectively, in the upper and in the lower row).

Figure 4

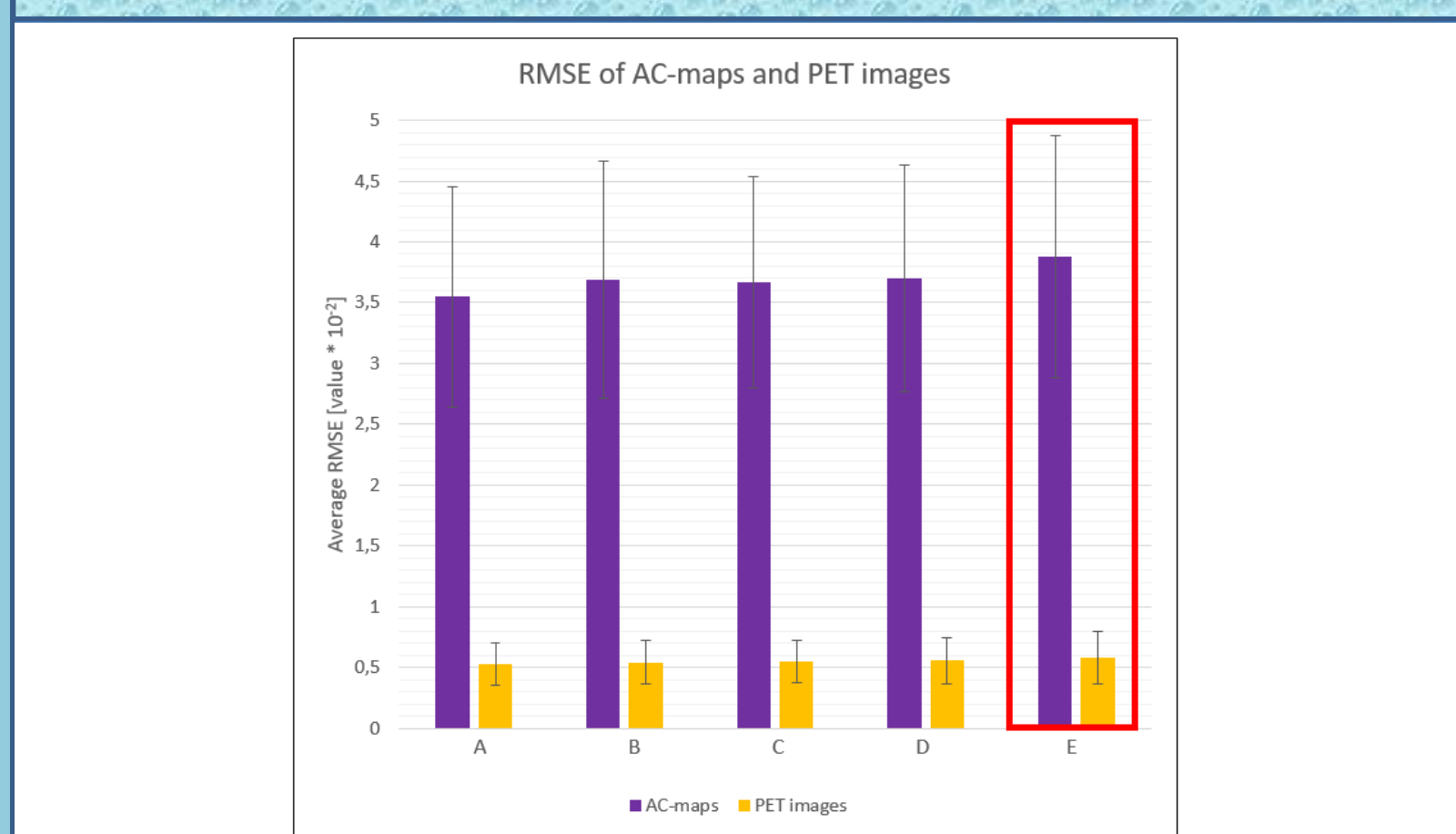


Fig. 4. RMSE of AC-maps and PET images. The red rectangle highlights the highest RMSE values.

Figure 5

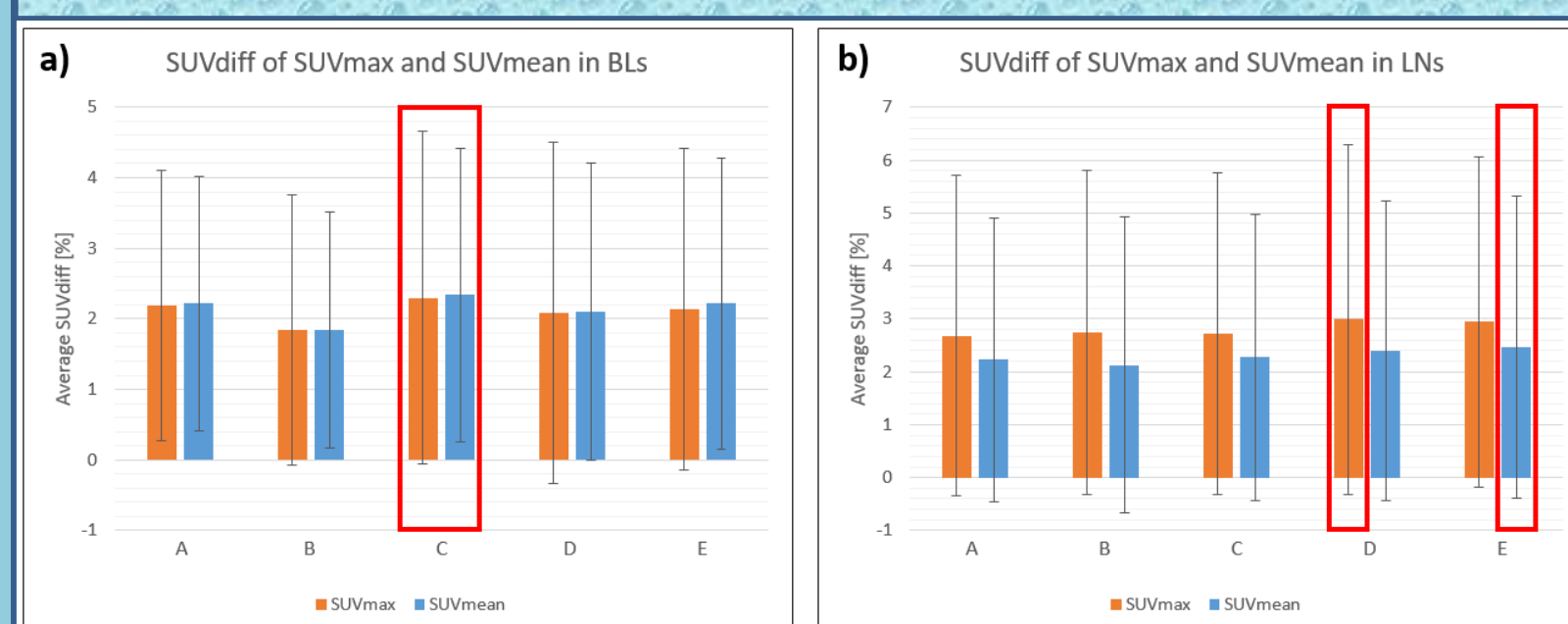


Fig. 5.  $SUV_{diff}$  of  $SUV_{max}$  and  $SUV_{mean}$  in BL (a) and LN (b). The red rectangles highlight the maximum values of  $SUV_{diff}$  of  $SUV_{max}$  and  $SUV_{mean}$  in BL and LN.

## RESULTS

Eighty-three lesions were identified: 46 BL and 37 active LN. Examples of AC-maps and final PET images with their voxel-wise subtraction between images obtained with different parameter set and the reference one are shown in Fig.2 and Fig.3. Fig.4 shows the RMSE of AC-maps and PET images. The RMSE calculation suggests that both for AC-maps and PET the highest differences are found between Ref and E) acquisitions ( $RMSE_{AC-map} = 3,88 \cdot 10^{-2} \pm 9,97 \cdot 10^{-3}$ ,  $RMSE_{PET} = 5,82 \cdot 10^{-3} \pm 2,17 \cdot 10^{-3}$ ). Fig.5 shows the  $SUV_{diff}$  of  $SUV_{max}$  and  $SUV_{mean}$  in BL (Fig.5a) and in LN (Fig. 5b) for the five reconstructions. For BL, C) shows the highest  $SUV_{diff}$  value for both  $SUV_{max}$  ( $2.3 \pm 2.36\%$ ) and  $SUV_{mean}$  ( $2.34 \pm 2.08\%$ ), while for axillary LN the highest differences are found in D) for  $SUV_{max}$  ( $2.99 \pm 3.31\%$ ) and in E) for  $SUV_{mean}$  ( $2.47 \pm 2.85\%$ ). Nevertheless, none of them is statistically significant.

## DISCUSSION AND CONCLUSIONS

From our results, spatial resolution and SNR acquisition parameter modifications in MRAC sequences seem to affect  $SUV_{mean}$  and  $SUV_{max}$  of the corresponding corrected PET images, but not significantly. Using improved shimming on the dorsal side has shown the highest effect on the RMSE both for AC-maps and for PET images.

## REFERENCES

- [1] A. Melsaether and L. Moy, "Breast PET/MR Imaging," Radiologic Clinics of North America, vol. 55, no. 3. pp. 579–589, 2017, doi: 10.1016/j.rcl.2016.12.001.
- [2] D. M. Plecha and P. Faulhaber, "PET/MRI of the breast," European Journal of Radiology, vol. 94. pp. A26–A34, 2017, doi: 10.1016/j.ejrad.2017.05.006.
- [3] C. Catana, "Principles of Simultaneous PET/MR Imaging," Magnetic Resonance Imaging Clinics of North America, vol. 25, no. 2. pp. 231–243, 2017, doi: 10.1016/j.mric.2017.01.002.
- [4] Y. Chen and H. An, "Attenuation Correction of PET/MR Imaging," Magnetic Resonance Imaging Clinics of North America, vol. 25, no. 2. pp. 245–255, 2017, doi: 10.1016/j.mric.2016.12.001.
- [5] J. M. Johnson, R. M. Strigel, L. C. H. Bancroft, A. M. Fowler, and A. B. McMillan, "Attenuation Correction Map Calculation and Truncation Completion for Breast PET/MR Imaging using Deep Learning," in Proc. Joint Annual Meeting ISMRM-ESMRMB, Paris, France 26, 2018, p. 4328.
- [6] I. Cho, E. Kong, and K. Chun, "Image artifacts from MR-based attenuation correction in dedicated PET/MR breast coil for PET/MR mammography," EJNMMI Phys., vol. 2, no. S1, 2015, doi: 10.1186/2197-7364-2-s1-a62.

## ACKNOWLEDGMENTS

This research was funded by Associazione Italiana per la Ricerca sul Cancro, grant number IG 2018 Id.21840 and Ministero della Salute Italiana (Italian Ministry of Health) for Ricerca Finalizzata Ordinaria, grant number RF-2018-12368096. Signa PET/MRI system (GE Healthcare, Waukesha, WI) used in the present work was purchased with funding from the Italian Ministry of Health.

Correspondence to:  
scifo.paola@hsr.it